A Velocity Form Model Predictive Control of an Autonomous Underwater Vehicle

Isah A. Jimoh *Student Member, IEEE* and Hong Yue, *Senior Member, IEEE*

Abstract—**This work presents a model predictive control (MPC) scheme to achieve three-dimensional (3D) tracking control and point stabilisation of an autonomous underwater vehicle (AUV) subject to environmental disturbances. The AUV is modelled as a coupled, nonlinear system. The control scheme is developed using a linear parameter-varying (LPV) formulation of the nonlinear model in velocity form to obtain an optimisation control problem with efficient online solvers and does not require model augmentation that can potentially increase computational efforts. The control strategy inherently provides offset-free control when tracking piece-wise constant reference signals, ensures feasibility for trajectories containing unreachable points and is relatively simple to implement since parameterisation of all equilibria is not required. A simple switching law is proposed for task switching between the 3D trajectory tracking and point stabilisation. The MPC is designed to ensure closed-loop stability of the vehicle in both motion control tasks via the imposition of terminal constraints. Through simulations of the coupled nonlinear Naminow-D AUV under ocean current and wave disturbances, the effectiveness of the control strategy in trajectory tracking and point stabilisation is demonstrated.**

Index Terms—**Model Predictive Control, Autonomous Underwater Vehicle, Trajectory Tracking, Positioning Control**

I. Introduction

In the past two decades, significant progress has been made in the field of autonomous underwater vehicles (AUVs), with a variety of results reported on its technological development [1], [2]. Applications are found in a wide range of tasks including ocean floor mapping, underwater structures inspection and maintenance, condition monitoring and survey, which highlights the need for AUV operation with some level of autonomy.

The operational duration of an AUV is limited by the internal battery which acts as the sole energy source. Remotely operated docking stations have been developed to avoid frequent launching and recovery tasks of the vehicle, enabling charging and data upload to be performed underwater [3]. Typically, two separate control problems are involved for AUV operation before retreating to the docking position, the trajectory tracking/path-following and the point stabilisation. The former entails the steering of the vehicle through a predefined track, the latter is on steering of the vehicle to a defined target position with a constant orientation [4]. These two control problems are mostly studied separately in the literature [4]–[6].

The authors are with the Wind Energy and Control Centre, Department of Electronic and Electrical Engineering, University of Strathclyde, Royal College Building, 204 George Street, Glasgow, Scotland, G1 1XW, United Kingdom. Emails: `isah.jimoh@strath.ac.uk`, `hong.yue@strath.ac.uk`.

An AUV is characterised by its high-dimensional, coupled, nonlinear dynamics with physical limitations, and its operation is subject to uncertain disturbance from marine environment. Motion controllers for underwater robots have been developed using classical modelling techniques such as input-output decoupling and local linearisation [7], which may fail to give satisfactory control performance as they are mainly suitable around a designated operating point or region. Other model-based approaches have been proposed to address the weaknesses of classical techniques. Backstepping based on Lyapunov theory is one of the commonly used nonlinear controllers for AUV motion control [4], [5], [8]. Environmental disturbances are either assumed to be known or estimated using a variety of methods such as exponential observer [9], neural networks [10] and fuzzy logic [11]. Some of these techniques require accurate models which are not easy to obtain [12].

Sliding mode control (SMC) has been proposed as an alternative technique for AUV control considering its high robustness to both model uncertainties and time-varying external disturbances [13]–[15]. A standard SMC has the drawback of making input chattering that may generate undesired high-frequency dynamics in motion control. Intelligent methods based on fuzzy logic have been deployed to reduce the effect of chattering in SMC [16], [17], with an increased complexity in controller design. Combined backstepping and SMC was proposed in [18]–[20], where backstepping is used to compute a virtual control law and SMC is employed to improve the overall robustness of the control system. In the context of backstepping SMC [21], unknown thrust dynamics was estimated using a recurrent neural network. A radial basis function neural network was used [22] to estimate uncertain model parameters and external disturbance to improve the performance of a backstepping terminal SMC scheme.

Recent AUV control strategies are aimed at addressing practical issues including system constraints [23]. There is no straightforward method of including system constraints in the control techniques described above. Model-based predictive control (MPC) provides a natural approach to incorporate constraints on inputs, states and outputs into controller design with robustness to system uncertainties [24], [25]. In [26], MPC was proposed for AUV control based on a model that is decoupled into the diving and manoeuvring planes. Two MPC controllers were used to control each plane separately. The input constraints were incorporated into the design, and the effects of external disturbances weren't considered. A Lyapunov-based nonlinear MPC (NMPC) law was proposed to handle coupling and nonlinearities in the AUV model

[23]. A robust nonlinear MPC scheme for AUV stabilisation with experimental validation was presented in [27]. A tube-based, collision-free tracking NMPC was developed based on a decoupled model, in which pitch and roll motions are neglected [28]. A challenge with NMPC schemes is their high computational cost which limits their potential for practical implementation. As a result, some studies [29] have focused on developing algorithms to speed up the control signal computation in NMPC framework for AUVs. In [30], a linearised AUV model was used to formulate a linear MPC based on a quadratic program with efficient off-the-shelf solvers. The scheme is not suitable for tracking curved trajectories since the nonlinearities of the vehicle will be amplified. More recently, a linear parameter varying (LPV) MPC (LPV-MPC) strategy based on the kinematic model of an AUV was proposed to track curved trajectories [31]. The study did not consider input torque and moment constraints [31]. In [32], an LPV-MPC was developed for the dynamic positioning of AUVs during docking and a Kalman filter was used to estimate modelling errors and external disturbances. Whereas theoretical stability proofs exist [23], [28] for AUV control systems based on NMPC, none of the studies [31], [32] based on LPV models provide theoretical proof for stability. Guaranteeing stability for LPV-MPC schemes for AUV control is challenging because they are required to track curved trajectories.

For AUVs with underwater docking stations, it is necessary to steer the vehicle during underwater operations through desired trajectories which may be curved before returning to the docking point where the vehicle needs to maintain a defined constant position for docking. In the literature discussed above, these problems are often studied differently because it is challenging to guarantee good performance in both curved and constant reference signal tracking. In the AUV context, tracking constant reference signals is known as *point stabilisation* which is closely related to dynamic positioning [4]. Since it is more challenging to track curved trajectories, many studies [23], [31] on AUV control have been dedicated to this task without necessarily considering how the proposed controllers would perform when tracking piece-wise constant signals under persistent disturbances such as ocean currents. When AUVs operate in relatively shallow waters, the effects of both ocean currents and waves need to be considered, which adds complexity to the controller design.

Considering the issues highlighted above, the main objective of this work is to develop an MPC scheme based on LPV formulation of the vehicle model that can effectively steer AUVs along 3D trajectories that may be curved, and also provide effective tracking of piece-wise constant reference signals required to maintain a desired position and orientation as in underwater docking operations. The main contributions of this paper are outlined below.

1) A novel velocity MPC algorithm without model augmentation is developed for a coupled and nonlinear AUV by reformulating its model as an LPV system. The key advantage of velocity MPC algorithm lies in its ability to provide offset-free control, particularly when tracking piece-wise constant reference signals. This capability is crucial for achieving effective point stabilization during docking operations, especially in the presence of unknown persistent disturbances. The conventional velocity MPC algorithms [33]–[35] are based on augmented models that lead to increased computational requirements due to increased state dimensions. Additionally, model augmentation may result in a loss of stabilisability. These issues had been reported [36] to be a limiting factor for the wide use of velocity MPC algorithm to high-order systems.

2) The velocity MPC problem is formulated to ensure nominal stability by satisfying the conditions of a defined reachable state. To smoothly transition from 3D trajectory tracking to point stabilisation and avoid jump discontinuity, a simple time parameterisation is proposed. This helps mitigate abrupt changes that could otherwise lead to infeasibility by necessitating substantial changes in input forces and velocities during the transition phase.

3) The developed AUV motion control scheme can cope with tracking reachable references and also trajectories including unreachable points. For AUVs operating in a constrained workspace, this feature can be used to ensure the AUV remains within the workspace boundaries that define the set of reachable output references.

The rest of this paper is organised as follows. Section II provides the modelling of AUV and environmental disturbances. In Section III, the velocity form LPV-MPC algorithm is developed and analysed. Section IV presents the simulation study and results. Concluding remarks and areas to be considered in future studies are discussed in Section V.

Notations

Hereafter, $\mathbb{N}$ denotes the non-negative integer set, $\mathbb{R}$ the real set, $\mathbb{R}^n$ and $\mathbb{R}^{m \times n}$ denote n-dimension vector and $m \times n$ matrix, $(\cdot)^\top$ denotes matrix transpose. $\mathbf{R} \succeq \mathbf{0}$ denotes a positive semi-definite real matrix. Given a vector $\mathbf{x} \in \mathbb{R}^n$ and a weighting matrix $\mathbf{Q} \in \mathbb{R}^{n \times n}$, the weighted 2-norm $\mathbf{x}^\top \mathbf{Q} \mathbf{x}$ is written as $\| \mathbf{x} \|_{\mathbf{Q}}^2$. The notations $\mathbf{I}_n$ and $\mathbf{0}_{m \times n}$ stand for an $n \times n$ identity matrix and an $m \times n$ zero matrix, respectively. The notation $\texttt{diag}(Q_1, \ldots, Q_n)$ denotes the block diagonal matrix having the entries $Q_1, \ldots, Q_n$ in its main diagonal. In addition, given $\mathbf{x} = [x_1 \ x_2, \ x_3]^\top$, we define the skew-symmetric matrix of $\mathbf{x}$ as $\mathbf{S}(\mathbf{x}) = \begin{bmatrix} 0 & -x_3 & x_2 \\ x_3 & 0 & -x_1 \\ -x_2 & x_1 & 0 \end{bmatrix}$.

II. AUV AND DISTURBANCE MODELLING

A. AUV Kinematics

The kinematic model forms the basis for the transformation from the vehicle's motion reference frame to the earth-fixed coordinate system. Whereas the earth-fixed reference frame is used to define the position and orientation of the vehicle, the motion reference frame is used to describe the velocities of the vehicle. The AUV kinematic model is written as

$$\dot{\boldsymbol{\eta}} = \mathbf{J}(\boldsymbol{\eta})\boldsymbol{\nu}, \tag{1}$$

in which

$$\mathbf{J}(\boldsymbol{\eta}) = \begin{bmatrix} \mathbf{J_1}(\boldsymbol{\eta}) & \mathbf{0_{3 \times 3}} \\ \mathbf{0_{3 \times 3}} & \mathbf{J_2}(\boldsymbol{\eta}) \end{bmatrix}$$
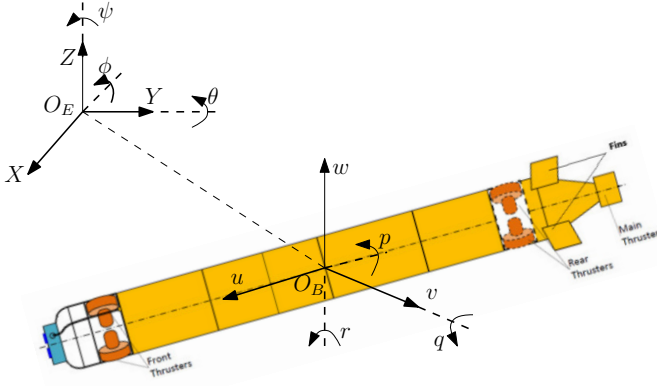
Fig. 1. Naminow-D AUV conceptual layout showing the 6 DoFs with body-fixed (O_B) and earth-fixed (O_E) reference frames illustrated

$$\mathbf{J_1(\eta)} = \begin{bmatrix} \cos\theta\cos\psi & -\sin\psi\cos\phi + \cos\psi\sin\theta\sin\phi \\ \sin\theta\cos\psi & \cos\psi\cos\phi + \sin\phi\sin\theta\sin\psi \\ -\sin\theta & \cos\theta\sin\phi \end{bmatrix}$$

$$\begin{array}{c} \cos\psi\cos\phi\sin\theta + \sin\psi\sin\phi \\ \sin\theta\sin\psi\cos\phi - \cos\psi\sin\phi \\ \cos\theta\cos\phi \end{array} \Bigg],$$

$$\mathbf{J_2(\eta)} = \begin{bmatrix} 1 & \sin\phi\tan\theta & \cos\phi\tan\theta \\ 0 & \cos\phi & -\sin\phi \\ 0 & \sin\phi/\cos\theta & \cos\phi/\cos\theta \end{bmatrix}.$$

Here, $\boldsymbol{\eta} = [x \; y \; z \; \phi \; \theta \; \psi]^\top$ is the vehicle's position vector in the earth-fixed reference frame, comprised of position (x, y, z) and orientation (ϕ, θ, ψ) variables. The roll angle, pitch angle and yaw angle are denoted by ϕ, θ and ψ. Also, $\boldsymbol{\nu} = [u \; v \; w \; p \; q \; r]^\top$ represents the vector of velocities, comprised of surge velocity u, sway velocity v, heave velocity w, roll rate p, pitch rate q and yaw rate r of the vehicle. A schematic diagram showing the 6 DoF of a typical streamlined underwater vehicle is shown in Fig. 1. Note that $\mathbf{J}(\boldsymbol{\eta})$ is singular for $\theta = \pm\pi/2$. Hence, we implement the constraint $|\theta| < \pi/2$ to prevent this singularity problem.

B. AUV Dynamics

The 6 DoF AUV motion dynamics that rely on the Newton-Euler equation and Quasi-Lagrange equation [7] can be written as

$$\mathbf{M}\dot{\boldsymbol{\nu}} + \mathbf{C}(\boldsymbol{\nu})\boldsymbol{\nu} + \mathbf{D}(\boldsymbol{\nu})\boldsymbol{\nu} + \mathbf{g}(\boldsymbol{\eta}) = \boldsymbol{\tau}, \qquad (2)$$

where the matrices $\mathbf{M}$, $\mathbf{C}(\boldsymbol{\nu})$, $\mathbf{D}(\boldsymbol{\nu})$ and $\mathbf{g}(\boldsymbol{\eta})$ are defined in Appendix V-A. The external forces and moments generated by the vehicle's thrusters are defined in a 6 DoF vector as

$$\boldsymbol{\tau} = [\tau_X \; \tau_Y \; \tau_Z \; \tau_K \; \tau_M \; \tau_N]^\top \in \mathbb{R}^{6\times 1}, \qquad (3)$$

with subscripts X, Y, Z, K, M, N used for each DoF. Their constraint sets are defined as follows:

$$\boldsymbol{\tau}_1 = [\tau_X \; \tau_Y \; \tau_Z]^\top \in \mathcal{T}_1 \subseteq \mathbb{R}^3, \qquad (4)$$

$$\boldsymbol{\tau}_2 = [\tau_K \; \tau_M \; \tau_N]^\top \in \mathcal{T}_2 \subseteq \mathbb{R}^3, \qquad (5)$$

for which we define

$$\mathcal{T}_1 := \left\{ \boldsymbol{\tau}_1 \in \mathbb{R}^3 : |\tau_X|, |\tau_Y|, |\tau_Z| \leq \tau_{1,\max} \right\}, \qquad (6)$$

$$\mathcal{T}_2 := \left\{ \boldsymbol{\tau}_2 \in \mathbb{R}^3 : |\tau_K|, |\tau_M|, |\tau_N| \leq \tau_{2,\max} \right\}. \qquad (7)$$

Here $\tau_{1,\max}$ and $\tau_{2,\max}$ denote upper bounds on the input forces and moments, respectively. The constraint set is

$$\mathcal{T} := \left\{ \tau \in \mathbb{R}^6 : |\tau| \leq \tau_{\max} \right\}, \qquad (8)$$

where $\tau = [\tau_1^\top \; \tau_2^\top]^\top$, $\tau_{\max} = [\tau_{1,\max}^\top \; \tau_{1,\max}^\top]^\top$.

C. Modelling the Effects of Environmental Disturbances

In this study, we consider the effects of external disturbances in the form of ocean currents and waves. Whereas ocean current $\boldsymbol{\nu}^c$ can be modelled as constant/slowly-changing disturbances that are irrotational in the inertia frame of reference [32], [37], ocean waves are time-varying in nature. Ocean currents are modelled as wave motion moving in a specified direction with an approximately constant speed affecting the vehicle's motion [38]. The assumption of irrotational currents implies that $p^c = q^c = r^c = 0 \, m/s$ while slowly-changing velocity of the currents mean that $\dot{u}^c = \dot{v}^c = \dot{w}^c \approx 0 \, m/s^2$. Therefore, ocean current is given by $\boldsymbol{\nu}^c = [u^c \; v^c \; w^c \; 0 \; 0 \; 0]^\top$.

Denote

$$\boldsymbol{\tau}^w = [\tau_X^w \; \tau_Y^w \; \tau_Z^w \; \tau_{KK}^w \; \tau_M^w \; \tau_N^w]^\top \in \mathbb{R}^{6\times 1} \qquad (9)$$

as the forces and moments generated by ocean waves affecting the vehicle's motion, with superscript 'w' standing for waves. Each component of the 6 DoFs ocean wave vector $\boldsymbol{\tau}^w$, can be modelled by a second-order system [7], i.e.,

$$\begin{bmatrix} \dot{z}_{i,1}^w \\ \dot{z}_{i,2}^w \end{bmatrix} = \begin{bmatrix} 0 & 1 \\ -\omega_{e,i}^2 & -2\xi_i\omega_{e,i} \end{bmatrix} \begin{bmatrix} z_{i,1}^w \\ z_{i,2}^w \end{bmatrix} + \begin{bmatrix} 0 \\ K_{w,i} \end{bmatrix} w_i \qquad (10)$$

$$\tau_i^w = \begin{bmatrix} 0 & 1 \end{bmatrix} \begin{bmatrix} z_{i,1}^w \\ z_{i,2}^w \end{bmatrix} + d_i \qquad (11)$$

where the subscript i ($= X$, Y, Z, K, M, N) corresponds to the DoF of the vehicle, the amplitude of $\boldsymbol{\tau}_i^w$ in the $i-$th DoF can be changed by the choice of parameter $K_{w,i}$. The term w_i is a zero-mean white process noise, ξ_i is the damping coefficient, $\omega_{e,i}$ is the frequency of encounter. It is noted $\omega_{e,i}$ is relevant only when the vehicle is moving at a forward speed $u > 0 \, m/s$. The term d_i in the output equation can be modelled as slowly changing bias terms (Wiener processes). It is recommended in [7] that a maximum value of $d_i^{\max}$ is applied to d_i, i.e., $|d_i| \leq d_i^{\max}$.

To simulate the effects of ocean currents and waves on the AUV motion, the model (2) is modified to obtain:

$$\mathbf{M}\dot{\boldsymbol{\nu}} + \mathbf{C}(\boldsymbol{\nu}^r)\boldsymbol{\nu}^r + \mathbf{D}(\boldsymbol{\nu}^r)\boldsymbol{\nu}^r + g(\boldsymbol{\eta}) = \boldsymbol{\tau} + \boldsymbol{\tau}^w, \qquad (12)$$

where $\boldsymbol{\nu}^r = \boldsymbol{\nu} - \boldsymbol{\nu}^c$ represents the relative velocity vector. Since the ocean current is generally constant or slowly-changing, it is assumed that the current acceleration is negligible, that is, $\dot{\boldsymbol{\nu}}^c \approx \mathbf{0}$. The model (12) is used to simulate the vehicle's motion while (2) is used for controller design.

III. PREDICTIVE CONTROL DESIGN

In this section, the design of a predictive controller is presented based on the LPV model of the AUV.

A. Problem Statement

Denote $\mathbf{x} = [\boldsymbol{\eta}^\top \ \boldsymbol{\nu}^\top]^\top \in \mathbb{R}^{12}$ as the state vector including the position vector, $\boldsymbol{\eta}$, and the velocity vector, $\boldsymbol{\nu}$. The kinematics and dynamics of an AUV can be combined to give the nonlinear state space model

$$\dot{\mathbf{x}} = \mathbf{A}_c(\mathbf{x}) + \mathbf{B}_c \boldsymbol{\tau} + \mathbf{D}_c \boldsymbol{\tau}^w,$$
$$\mathbf{y} = \mathbf{G}\mathbf{x}, \tag{13}$$

in which

$$\mathbf{A}_c(\mathbf{x}) = \begin{bmatrix} \mathbf{0} & \mathbf{J}(\boldsymbol{\eta}) \\ \mathbf{0} & -\mathbf{M}^{-1}(\mathbf{C}(\boldsymbol{\nu}^r) + \mathbf{D}(\boldsymbol{\nu}^r)) \end{bmatrix} \mathbf{x} - \begin{bmatrix} \mathbf{0} \\ \mathbf{M}^{-1}(\mathbf{g}(\boldsymbol{\eta})) \end{bmatrix},$$

$$\mathbf{B}_c = \begin{bmatrix} \mathbf{0} \\ \mathbf{M}^{-1} \end{bmatrix}, \mathbf{D}_c = \begin{bmatrix} \mathbf{0} \\ \mathbf{M}^{-1} \end{bmatrix}, \mathbf{G} = [\mathbf{I} \ \mathbf{0}],$$

and $\mathbf{y} = \boldsymbol{\eta} \in \mathbb{R}^6$ is the output vector. A constraint is applied on the position vector $\boldsymbol{\eta}$ to avoid singular transformation matrix $\mathbf{J}(\boldsymbol{\eta})$. Moreover, it is desired that the linear velocities of the underwater vehicle have an upper bound since most tasks are performed at relatively low speeds [27]. Hence, the constraint set $\mathcal{X}$ for the state vector is defined as

$$\mathcal{X} := \left\{ \mathbf{x} \in \mathbb{R}^{12} : |\mathbf{x}| \le \mathbf{x}_{\max} \right\}, \tag{14}$$

where $\mathbf{x}_{\max}$ defines a hard constraint on the state vector.

Assume a smooth time-dependent trajectory

$$\mathbf{y}^d(k) = [x^d(k) \, y^d(k) \, z^d(k) \ \phi^d, \theta^d, \psi^d]^\top, \tag{15}$$

the problem considered in this work includes two tasks:

1) 3D tracking. Steer the AUV, modelled by the nonlinear, coupled model in (13), for $x(k)$, $y(k)$ and $z(k)$ to follow $[x^d(k) \, y^d(k) \, z^d(k)]^\top$ until the AUV reaches the docking vicinity. The orientation variables, $\phi(k)$, $\theta(k)$ and $\psi(k)$, do not need to track any desired references during this task period.

2) Point stabilisation. When the AUV reaches the docking vicinity, the objective here is to maintain the vehicle at the desired position and orientation, $\mathbf{y}_s^d = [x_s^d \, y_s^d \, z_s^d \ \phi^d \ \theta^d \ \psi^d]^\top$. The reference at steady state is denoted as $\mathbf{y}_s^d$.

These two control objectives need to be achieved while ensuring

- the capability to minimise the impact of environmental disturbances and model mismatch during trajectory tracking;
- the AUV is able to achieve the desired position and orientation for docking via the integral action in the MPC controller;
- the physical limitations in the form of input saturation for forces and moments and state constraints for pitch angle and linear velocities are satisfied;
- the vehicle can track both reachable and unreachable reference signals.

B. Novel MPC Design

The continuous nonlinear model in (13) is simplified by setting $\mathbf{g}(\boldsymbol{\eta}) = \mathbf{0}$, neglecting the unknown ocean currents and waves and discretised by applying the Forward Euler method

to give the LPV state space model for control design.

$$\mathbf{x}(k+1) = \mathbf{A}_\mathbf{x}\mathbf{x}(k) + \mathbf{B}\boldsymbol{\tau}(k)$$
$$\mathbf{y}(k) = \mathbf{G}\mathbf{x}(k) \tag{16}$$

where

$$\mathbf{A}_\mathbf{x} = \begin{bmatrix} \mathbf{I} & \mathbf{J}(\boldsymbol{\eta})T_s \\ \mathbf{0} & (\mathbf{I} - \mathbf{M}^{-1}(\mathbf{C}(\boldsymbol{\nu}) + \mathbf{D}(\boldsymbol{\nu})))T_s \end{bmatrix},$$

$$\mathbf{B} = \begin{bmatrix} \mathbf{0} \\ \mathbf{M}^{-1}T_s \end{bmatrix},$$

in which T_s is the sampling time and k is time index. For simplicity of notation, the time index in $\boldsymbol{\eta}$ and $\boldsymbol{\nu}$ are omitted in the definition of $\mathbf{A}_\mathbf{x}$ since they correspond to that of $\mathbf{x}(k)$.

To reduce the impact of the modelling errors and external disturbances, the velocity form of MPC is considered. Specifically, a new formulation of the optimisation problem is employed where the state augmentation can be avoided. First, write the increment form of the LTV model as

$$\Delta\mathbf{x}(k+1) = \mathbf{A}_\mathbf{x}\Delta\mathbf{x}(k) + \mathbf{B}\Delta\boldsymbol{\tau}(k)$$
$$\mathbf{y}(k) = \mathbf{G}\Delta\mathbf{x}(k) + \mathbf{y}(k-1) \tag{17}$$

where $\Delta\mathbf{x}(k) = \mathbf{x}(k) - \mathbf{x}(k-1)$, $\Delta\boldsymbol{\tau}(k) = \boldsymbol{\tau}(k) - \boldsymbol{\tau}(k-1)$, and there is an implicit velocity term $\Delta\nu(k) = \nu(k) - \nu(k-1)$.

The following assumptions are made for the LTV model.

Assumption 1.

1) The sets defined by the constraints $\mathcal{X}$ in (14) and $\mathcal{T}$ in (8) are convex sets containing the origin.
2) Model (16) is locally stabilisable for all $\mathbf{x}(k) \in \mathcal{X}$.

It is worth noting that trajectory generation algorithms typically produce smooth paths for navigation [7]. However, the transition towards the docking point specified by $\mathbf{y}_s^d$ may result in a jump discontinuous reference signal. This can be addressed by parameterising the straight line joining the final point of the trajectory to the docking position. This may be done by defining $\mathbf{p}_t(k) = [x_t \ y_t \ z_t]^\top$ as the tail of the smooth trajectory (15) and $p_s = [x_s^d \ y_s^d \ z_s^d]^\top$. The transition must be performed at a low resultant speed defined as $U_s = \sqrt{u^2 + v^2 + w^2}$. Based on this, the transition time t_s can then be approximated as

$$t_s = \frac{\| p_t - p_s \|}{T_s U_s}. \tag{18}$$

Note that the definition of (18) assumes the desired trajectory and the AUV model are sampled using the same period. Define $h = m/t_s$ with $m = 1, 2, 3 \ldots$, then, the parameterisation is obtained as

$$\mathbf{p}_s^d(k) = \begin{cases} (h-1)\mathbf{p}_t(k) + h\mathbf{p}_s^d, & \text{if } h \le 1 \\ \mathbf{p}_s^d, & \text{Otherwise} \end{cases} \tag{19}$$

where $p_s(k) = [x_s^d(k) \ y_s^d(k) \ z_s^d(k)]^\top$. Through (19), a smooth transition from the 3D trajectory to the docking point can be achieved since $\mathbf{y}_s^d$ is replaced by the time-parameterised reference signal defined by $\mathbf{y}_s^d(k) = [x_s^d(k) \ y_s^d(k) \ z_s^d(k) \ \phi^d \ \theta^d \ \psi^d]^\top$.

Several velocity/increment MPC algorithms have been developed for linear and nonlinear systems [34], [35], [39],
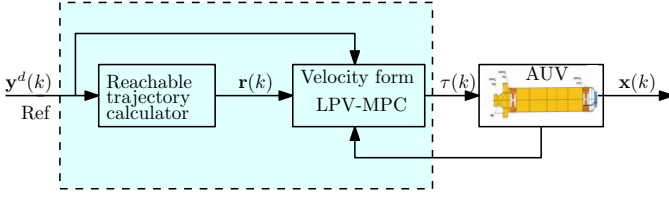
Fig. 2. Control strategy leveraging reachable references and velocity dynamics

[40]. The nonlinear method in [35] leads to a quasi-LPV MPC. The state velocity is augmented with the outputs of the system and used as the prediction model. Such a method increases the dimension of the prediction model from $\mathbb{R}^{12}$ to $\mathbb{R}^{18}$, leading to increased computational cost. Moreover, the stabilisability of the augmented model may not be locally guaranteed even when the original system $(\mathbf{A_x}, \mathbf{B})$ is locally stabilisable since there would be a need to ensure that the original system has no zero at the origin. In this work, we propose a different approach in the implementation of the velocity MPC, with the aim to achieve the tracking capability without applying state augmentation.

Define the set of reachable states in N steps as

$$\mathcal{R}_{\mathcal{X}}^N = \{\mathbf{x}_r(k) \mid \exists(\Delta\boldsymbol{\tau}(k|k), \ldots, \Delta\boldsymbol{\tau}(N-1|k):$$
$$\Delta\mathbf{x}(k+j|k) = \mathbf{A_x}\Delta\mathbf{x}(k|k) + \sum_{i=0}^{j-1}\mathbf{A_x}^i\mathbf{B}\Delta\boldsymbol{\tau}(k+i|k),$$
$$\mathbf{x}(k+N|k) = \mathbf{x}_r(k), \; \mathbf{x}(k+j|k) \in \mathcal{X},$$
$$\boldsymbol{\tau}(k+j-1|k) = \boldsymbol{\tau}(k-1) + \sum_{i=0}^{j-1}\Delta\boldsymbol{\tau}(k+i|k) \in \mathcal{U}$$
$$\Delta\boldsymbol{\nu}(k+N|k) = \mathbf{0}, \; j = 1, \ldots, N\}$$

The corresponding reachable output set is denoted by $\mathcal{R}_{\mathcal{Y}}^N$. For workspace constrained AUV operation, the linear position variables, (x, y, z), may become unreachable. To avoid this, define $\mathbf{r} \in \mathcal{Y}_r$, in which $\mathcal{Y}_r \subseteq \mathcal{Y}$ denotes the set that incorporate the workspace positional constraints. Then, the set for reachable output reference signal is defined as

$$\mathcal{R}_{\mathcal{Y}} = \left\{\mathbf{r} \in \mathcal{R}_{\mathcal{Y}}^N \mid \lambda\mathbf{r} + (1-\lambda)\mathbf{y}(k) \in \mathcal{R}_{\mathcal{Y}}^N, \mathbf{r} \in \mathcal{Y}_r\right\},$$

where $0 \leq \lambda \leq 1$ is a constant coefficient, ensuring $\mathbf{r}$ and $\mathbf{y}(k)$ belong to the same convex set of $\mathcal{R}_{\mathcal{Y}}^N$. Then, the reachable reference trajectory in every time step $\mathbf{r}(k)$, is computed by solving the problem

$$\mathbf{r}(k) = \arg\min_{\mathbf{r}\in\mathcal{R}_{\mathcal{Y}}} \| \mathbf{r} - \mathbf{y}^d(k) \|_{\mathbf{P}}^2 \tag{20}$$

with $\mathbf{P} \succ \mathbf{0}$. Given the desired trajectory $\mathbf{y}^d(k)$ in (15), the following cost function is considered

$$V(\mathbf{r}(k), \mathbf{Y}(k), \Delta\mathbf{U}(k))$$
$$= \sum_{j=1}^{N-1} \| \mathbf{r}(k) - \mathbf{y}(k+j|k) \|_{\mathbf{Q}}^2 + \sum_{i=0}^{N-1} \| \Delta\boldsymbol{\tau}(k+i|k) \|_{\mathbf{R}}^2 \tag{21}$$

where $\Delta\mathbf{U}(k) = [\Delta\boldsymbol{\tau}(k|k)^\top \; \ldots \; \Delta\boldsymbol{\tau}(k+N_u-1|k)^\top]^\top$ and $\mathbf{Y}(k) = [\mathbf{y}(k+1|k)^\top \; \ldots \; \mathbf{y}(k+N-1|k)^\top]^\top$, $\mathbf{Q} \succ \mathbf{0}$ and $\mathbf{R} \succ \mathbf{0}$ are the weighting matrices for output tracking and control activities, respectively.

The proposed MPC is formulated as a finite-horizon constrained optimal control problem using the velocity form prediction model (17). Considering a quadratic cost function, the novel velocity form MPC problem is formulated as

$$\Delta\mathbf{U}(k)^* = \arg\min_{\Delta\mathbf{U}(k)} V(\mathbf{r}(k), \mathbf{Y}(k), \Delta\mathbf{U}(k))$$

s.t :
$$\mathbf{y}(k+j|k) = \mathbf{C}\Delta\mathbf{x}(k+j|k) + \mathbf{y}(k+j|k-1)$$
$$\Delta\mathbf{x}(k+j|k) = \mathbf{A_x}^j\Delta\mathbf{x}(k|k) + \sum_{i=0}^{j-1}\mathbf{A_x}^i\mathbf{B}\Delta\boldsymbol{\tau}(k+i|k)$$
$$\mathbf{x}(k+j|k) \in \mathcal{X}, \; j = 1, \ldots, N,$$
$$\boldsymbol{\tau}(k+i|k) \in \mathcal{T}, \; i = 0, \ldots, N-1,$$
$$\Delta\mathbf{x}(k|k) = \Delta\mathbf{x}(k)$$
$$\mathbf{y}(k+j|k-1) = \mathbf{y}(k-1)$$
$$\mathbf{y}(k+N|k) = \mathbf{r}(k), \; \Delta\boldsymbol{\nu}(k+N|k) = \mathbf{0}$$
$$\tag{22}$$

where N is the prediction horizon, and $\Delta\mathbf{U}(k)^* = \{\Delta\boldsymbol{\tau}(k|k)^*, \ldots, \Delta\boldsymbol{\tau}(k+N_u-1|k)^*\}$ is the optimal control sequence. It is noted that obtaining the control sequence by solving (22) satisfies the reachable set requirement and assures that the AUV's prescribed trajectory does not exceed the workspace boundary. Furthermore, the constraints defined as $\mathbf{y}(k+N|k) = \mathbf{r}(k)$ and $\Delta\boldsymbol{\nu}(k+N|k) = \mathbf{0}$ are enforced to impose stability. For every time step k, the stability constraint ensures that the reachable state is given as $\mathbf{x}_r(k) = [\mathbf{r}(k)^\top \; \boldsymbol{\nu}(k+N-1|k)^\top]^\top$. They are set up to assure that the terminal state in each N-window, $\mathbf{x}(k+N|k)$, is a forced equilibrium when the reference $\mathbf{r}(k)$ is constant during point stabilisation task as the AUV navigates at a constant speed. For time-varying reference signal $\mathbf{r}(k)$, these constraints ensure $\mathbf{x}(k+N|k)$ is always feasible because $\mathbf{r}(k)$ is defined within the reachable set according to (20). Based on the receding horizon strategy, the optimal input increment at k is $\Delta\boldsymbol{\tau}(k|k)^*$ and the corresponding control input applied is

$$\boldsymbol{\tau}(k) = \boldsymbol{\tau}(k-1) + \Delta\boldsymbol{\tau}(k|k)^* \tag{23}$$

The control strategy leveraging the concept of reachable set is depicted in Fig. 2.

Denote $\mathbf{Q}_1 \in \mathbb{R}^{6\times6}$ and $\mathbf{Q}_2 \in \mathbb{R}^{6\times6}$ as two diagonal matrices on the output error weighting, used for the 3D trajectory tracking and the point stabilisation for docking, respectively. For the trajectory tracking problem, the weighting priorities are put on minimisation of the three error terms on linear positioning

$$e_x(k) = x^d(k) - x(k), \; e_y(k) = y^d(k) - y(k),$$
$$e_z(k) = z^d(k) - z(k). \tag{24}$$

For point stabilisation, the setting of $\mathbf{Q}_2$ needs to cover all 6 DoFs, that is, in addition to the three errors in (24), the following three orientation errors

$$\mathbf{e}_\phi(k) = \phi^d - \phi(k), \; e_\theta(k) = \theta^d - \theta(k),$$
$$e_\psi(k) = \psi^d - \psi(k), \tag{25}$$

also need to be minimised so that the specified linear position and orientation are maintained. Switching between the use of

---

Algorithm 1: MPC for 3D trajectory tracking and point stabilisation

---

Input: AUV LPV model, $\mathbf{Q}$, $\mathbf{R}$, N and N_u with $N_u < N$.

1 Define the transition resultant speed U_s.

2 Implement (19) to assure smooth transition from trajectory tracking to point stabilisation.

3 **for** $k \geq 0 \in \mathbb{N}$ **do**

4   **if** $\Delta \mathbf{y}^d(k)/T_s = \mathbf{0}$ **then**

5       $\mathbf{Q} = \mathbf{Q}_2$

6   **else**

7       $\mathbf{Q} = \mathbf{Q}_1$

8   **end**

9   Solve (20) to obtain $\mathbf{r}(k)$

10   Get $\Delta \mathbf{x}(k)$ and $\mathbf{y}(k-1)$; then, solve (22).

11   Obtain the optimal input $\boldsymbol{\tau}(k)$ based on (23).

12   Apply input to the AUV to obtain $\mathbf{x}(k+1)$

13   $k \leftarrow k+1$

14 **end**

$\mathbf{Q}_1$ and $\mathbf{Q}_2$ depends on the nature of the reference signal, $\mathbf{y}^d(k)$. When $\mathbf{y}^d(k)$ is time-varying, $\mathbf{Q} = \mathbf{Q}_1$ holds; when $\mathbf{y}^d(k)$ is time-invariant, $\mathbf{Q} = \mathbf{Q}_2$ is applied. With sampling time of T_s, $\Delta \mathbf{y}^d(k)/T_s \neq \mathbf{0}$ for time-varying $\mathbf{y}^d(k)$, and for time-invariant reference, $\Delta \mathbf{y}^d(k)/T_s = \mathbf{0}$. The implementation procedure for the developed predictive controller is outlined in Algorithm 1. It is noted that the proposed algorithm imposes a computational burden similar to that of a standard MPC problem, with the only extra demand being the solution of (20), which constitutes a relatively straightforward quadratic problem. Consequently, this approach allows us to avoid the need to solve a high-dimensional nonlinear MPC problem having both state and input constraints. Nevertheless, we acknowledge significant advancements that have been achieved in expediting computations within the realm of nonlinear MPC [29], [41].

Remark 1. *The stability constraint is employed to theoretically demonstrate that the MPC problem (22) ensures stability for the discretised model (17). Enforcing this constraint typically means using a longer prediction horizon compared to scenarios where the constraint is overlooked.*

C. Offset-free Control and Stability Analysis

Let $\mathbf{d}(k)$ represent the lumped unknown disturbances affecting the vehicle, including both constant and time-varying components. The convergence of the system states is a necessary assumption to assure the offset-free property of an MPC controller [42]. The states and outputs of the closed-loop system converge to steady state values as $k \to \infty$, $\mathbf{y}^d(k) \to \mathbf{y}_s^d$.

Remark 2. *Although tracking error may not be completely eliminated under time-varying disturbances and reference signals, a well-posed optimisation problem can help to minimise the tracking error. Moreover, it is desirable to achieve offset*

elimination subject to the constant or slowly-varying disturbances during docking so as to ensure that the vehicle is driven as close as possible to the desired position and orientation.

The following theorem summarises the main properties of the proposed control strategy.

Theorem 1. *Under Assumption 1, the control law $\boldsymbol{\tau}(k)$, obtained by solving (22), starting from a feasible initial state increment $\Delta \mathbf{x}(0)$, and applying (23), is recursively feasible and stabilises system (17). As $k \to \infty$, this controller makes the output converge to one of the following: (i) $\mathbf{y}_s^d$ if $\mathbf{y}_s^d \in \mathcal{R}_{\mathcal{Y}}$; (ii) $\mathbf{r}(k)$ if $\mathbf{y}_s^d \notin \mathcal{R}_{\mathcal{Y}}$, where $\mathbf{r}(k)$ is obtained by solving (20).*

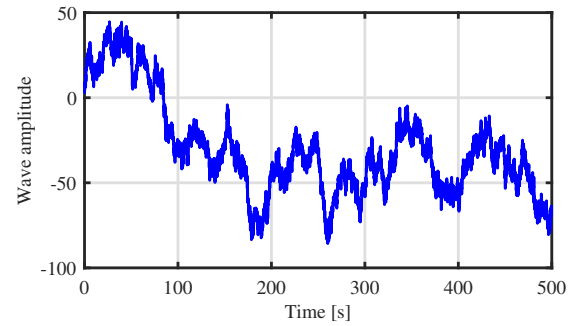*Proof.* See Appendix V-B for the proof of the theorem. □

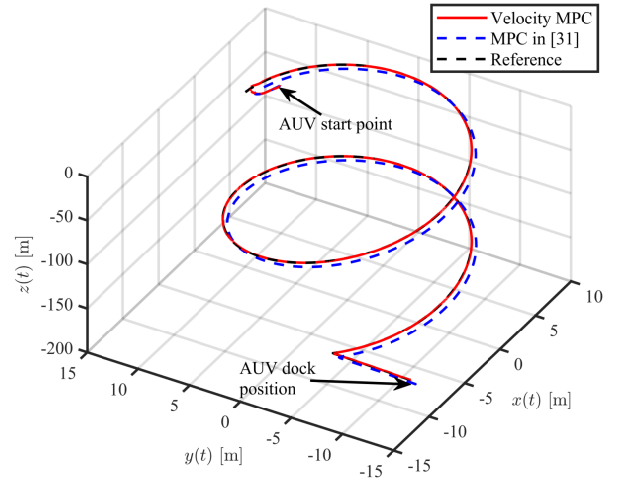Fig. 3. Wave signal produced using modified Pierson–Moskowitz Spectrum

Fig. 4. Case 1: AUV 3D closed-loop response for combined trajectory tracking and point stabilisation control.

TABLE I
NAMINOW-D AUV DYNAMIC PARAMETERS

$X_{\dot{u}}$	$Y_{\dot{v}}$	$Z_{\dot{w}}$	$Y_{\dot{r}}$	$Z_{\dot{q}}$	$M_{\dot{w}}$	$N_{\dot{v}}$
-6	-230	-230	28.3	-28.3	-28.3	28.3
$K_{\dot{p}}$	$M_{\dot{q}}$	$N_{\dot{r}}$	$X_{\|u\|u}$	$Y_{\|v\|v}$	$Z_{\|w\|w}$	$K_{\|p\|p}$
-1.31	-161	-161	-12.7	-574	-574	-0.63
$M_{\|q\|q}$	$N_{\|r\|r}$	$Y_{\|r\|r}$	$Z_{\|q\|q}$	$M_{\|w\|w}$	$N_{\|v\|v}$	m
-4127	-4127	12.3	12.3	27.4	-27.4	197.8
W	B	x_b	y_b, z_b	I_{xx}	I_{yy}	I_{zz}
1940	1999	-1.378	0	5.8	144	114

TABLE II
CONTROLLERS TURNING PARAMETERS

Parameter	Notation	MPC [31]	Proposed MPC
Prediction horizon	N	20	20
Control weights	$\mathbf{R}$	$20\mathbf{I}$	$0.05\mathbf{I}$
Output weights	$\mathbf{Q}$	$\mathbf{I}$	–
Output weight for objective 1	$\mathbf{Q}_1$	–	$\texttt{diag}(2, 2, 2, 1, 1, 1) \times 1000$
Output weight for objective 2	$\mathbf{Q}_2$	–	$1000\mathbf{I}$
Weight in (20)	$\mathbf{P}$	–	$\mathbf{I}$

IV. SIMULATED CASE STUDIES

A. Simulation Set-up

The wave model in (10) and (11) is considered in approximating first- and second-order components of ocean waves.

Here, we employ the modified Pierson–Moskowitz Spectrum [7] with $\xi_i = 0.2573$ and $\omega_{e,i} = 0.8$ rad/s under beam sea condition. The gain $K_{w,i} = 1.5$ and w_i is modelled as a white process noise with zero mean and standard deviation of 0.15. Furthermore, d_i is modelled as a standard Wiener process in the range $[-100, 100]$. These parameters are assumed to hold for $i = X, Y, Z, K, M, N$, i.e., the wave is considered the same in all 6 DoFs. The ocean current is modelled in the Cartesian plane with $u^c = 0.2$ m/s, $v^c = 0.15$ m/s, $w^c = 0.1$ m/s. In the studied scenario, the dynamics of the AUV are considered to be affected by both ocean currents and waves according to (13). The wave signal impacting the six DoFs of the AUV dynamics is shown in Fig. 3.

The Naminow-D dynamic parameters first published in [32] are given in Table I. A state constraint is implemented on the pitch angle such that $|\theta| < \pi/2$ always hold. Since in many
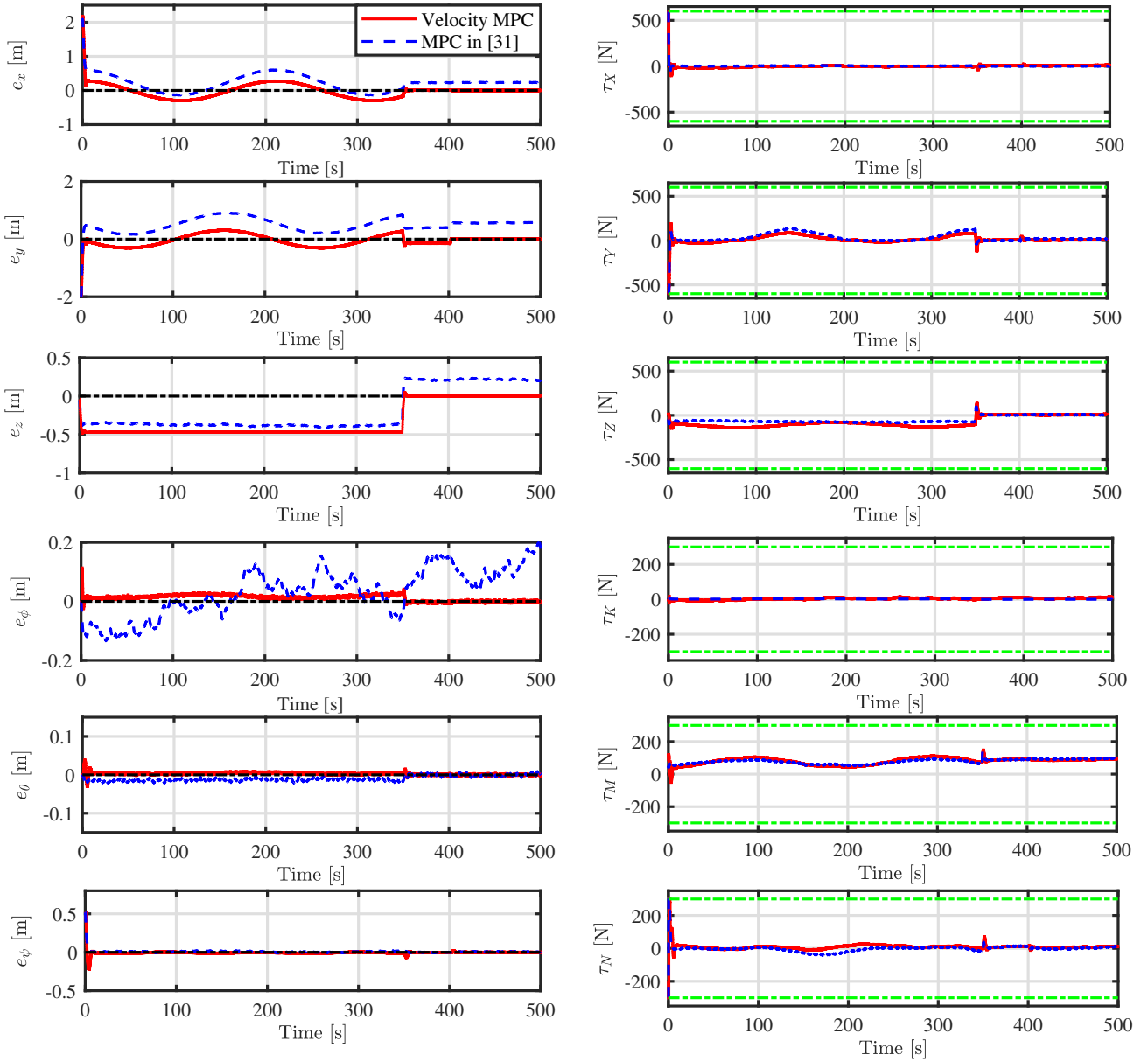

Fig. 5. Case 1: Evolution of errors (left) and input forces and moments (right). The green lines in the selected input plot show their constraints.
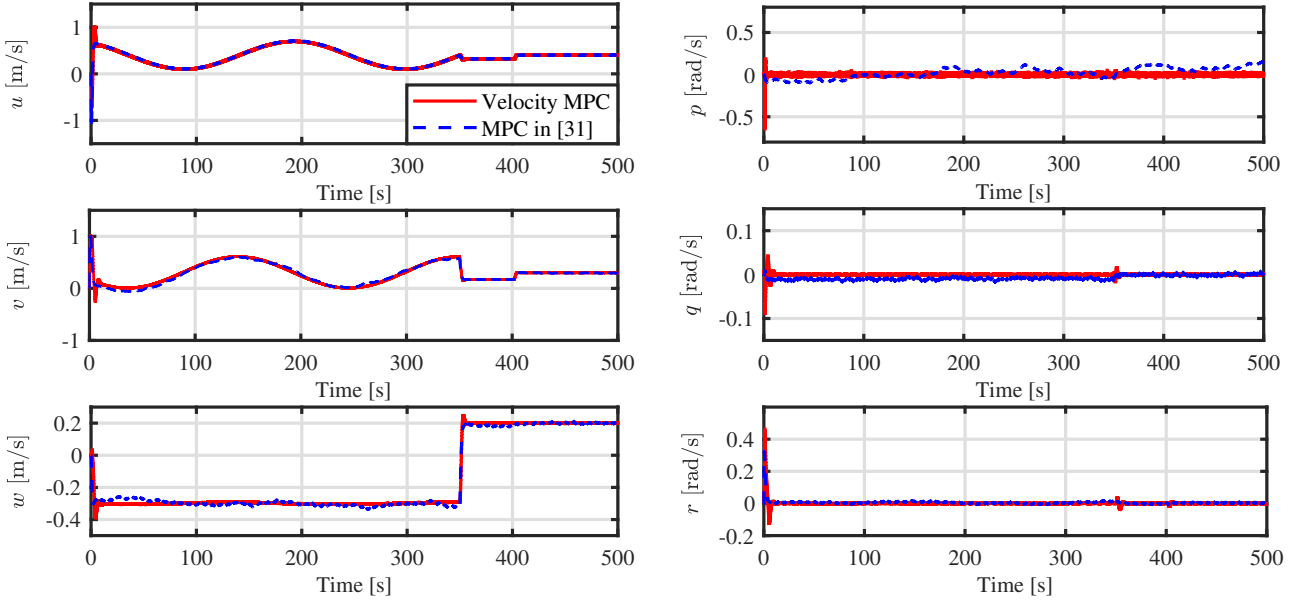
Fig. 6. Case 1: Evolution of linear (left) and angular (right) velocities of the AUV.

underwater tasks AUVs are required to move at relatively low speeds [27], we define upper bounds on the linear velocities: $u_{\max} = 1.5$ m/s, $v_{\max} = 1$ m/s and $w_{\max} = 0.5$ m/s. The input forces and moments are constrained as follows: $\boldsymbol{\tau}_{1,\max} = [600\ 600\ 600]^\top$ N and $\boldsymbol{\tau}_{2,\max} = [300\ 300\ 300]^\top$ Nm.

The parameter setting for the proposed MPC and the MPC from [31] are shown in Table II. The same prediction horizon is used for the two controllers. The weights on the linear position terms in $\mathbf{Q}_1$ are selected to be twice of those in $\mathbf{Q}_2$ to prioritise minimisation of the linear position errors during trajectory tracking control. The simulation experiment was set up in `MATLAB` environment where (20) and (22) are solved using `quadprog` to obtain the control signals applied to the nonlinear model (13).

B. Simulation Results

1) Case 1: The 3D reference trajectory is defined as

$$\mathbf{y}^d(t) = [10\sin0.03t\ \ 10\cos0.03t\ -0.5t\ \ 0\ \ 0\ \ \pi/6]^\top, t \le 350 \text{ s}$$
(26)

and the final docking position is

$$\mathbf{y}_s^d = [-9.0\ -12\ -175\ \ 0\ \ 0\ \ \pi/6]^\top, t > 350 \text{ s}, \quad (27)$$

where $t = kT_s$. Notice that the AUV needs to perform the task with a $30°$ heading angle. Also, it is generally desired to always keep roll motion, $(\phi,\ p)$, minimal for improved stability of marine vehicles [43]. Since the final point on the trajectory (26) is significantly distant from the docking position (27), the straight line joining these points is paramterised by considering a resultant AUV speed of $U_s = 0.15$ m/s. When the vehicle approaches the docking point defined at $t \ge 350$ s, it is essential to control the AUV's linear and angular positions such that the errors in the 6 outputs is as small as possible for effective docking operation.

The AUV's initial position is $\boldsymbol{\eta}(0) = [2\ 8\ 0\ 0\ 0\ 0]^\top$. The 3D motion profiles of the Naminow-D AUV along with

the defined trajectory for the two predictive controllers are shown in Fig. 4. Fig. 5 shows the time profiles of the position tracking errors and input signals for both control methods, from which it is seen that the proposed controller provides better tracking performance. In the second phase when the vehicle is driven towards the docking position, the merit of the proposed controller is even more evident. With MPC in [31], steady state errors are maintained due to the persistent non-zero disturbances, whereas the proposed MPC achieves
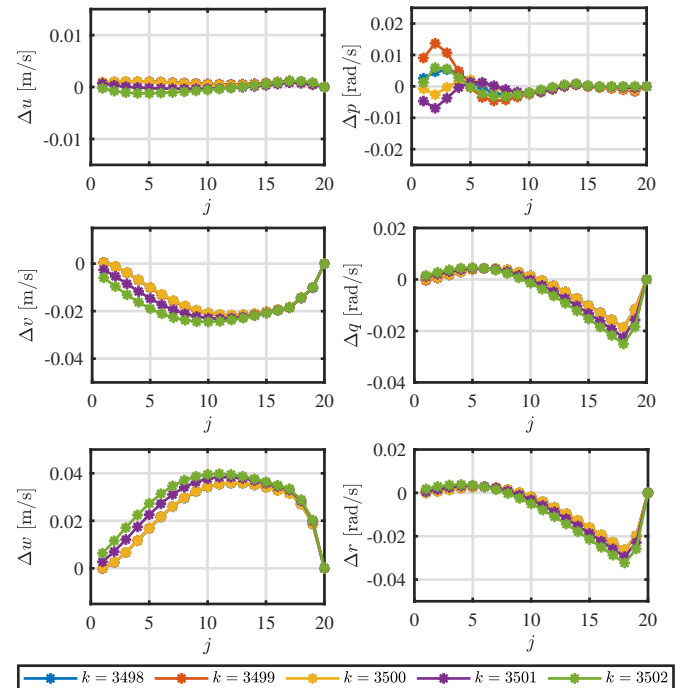

Fig. 7. Case 1: Predicted velocity increment trajectories at selected time instants.
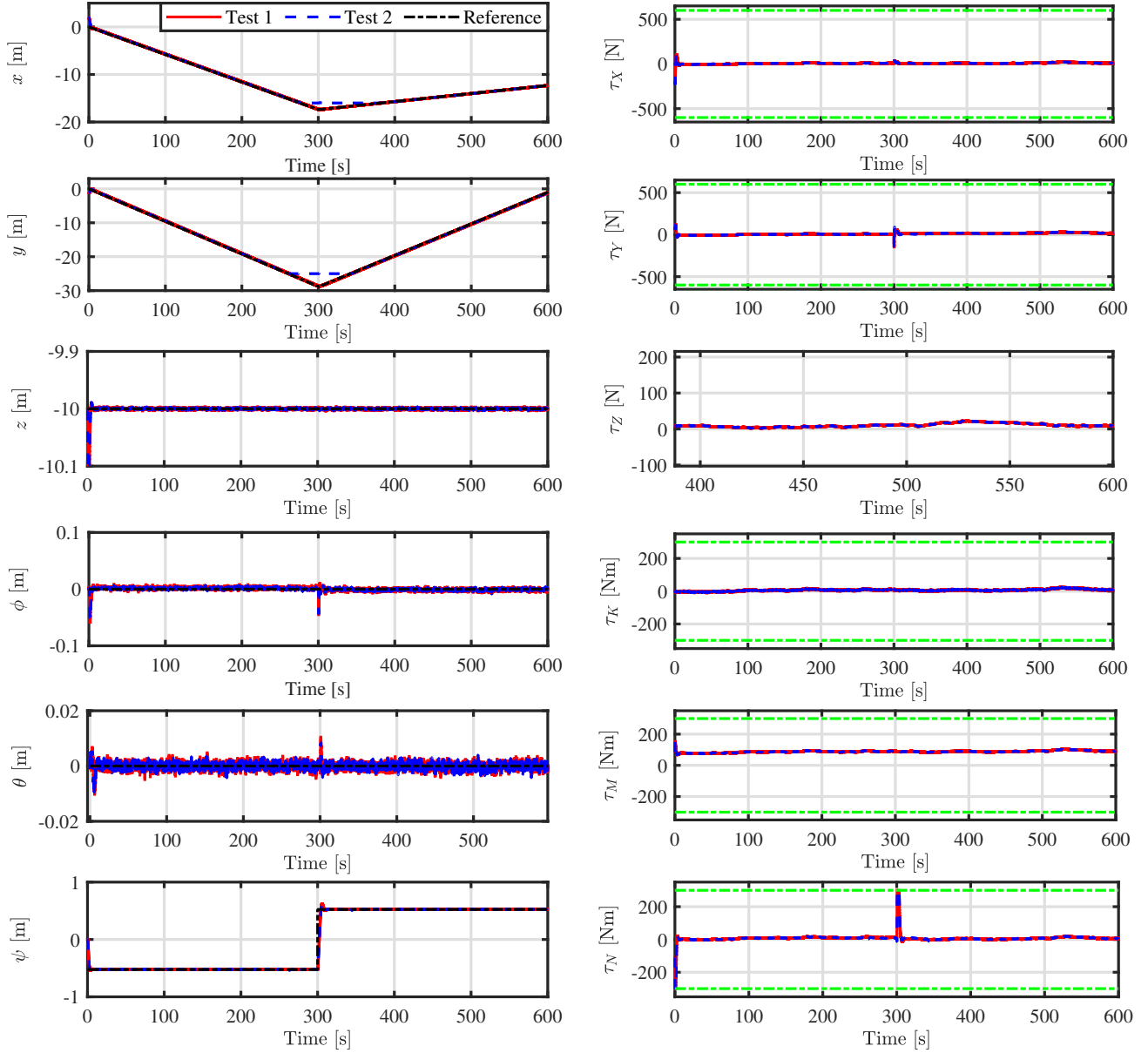
Fig. 8. Case 2: Closed-loop response under Test 1 and Test 2. Green lines show input constraints.

the docking position with close-to-zero errors in all 6 DoFs. The linear and angular velocities of the AUV are shown in Fig. 6. A salient point worthy of note is that the linear velocities do not converge to zeros at the docking point because the AUV needs to maintain speeds that counter the effects of the non-zero linear velocities of ocean currents $\boldsymbol{\nu}^c$. When compared to the results from the MPC in [31], the proposed MPC provides better stabilisation of roll motion by keeping the roll angle ϕ, and velocity p, in the vicinity of zero. Therefore, the results show the superiority of the proposed MPC in 3D trajectory tracking and point stabilisation control tasks. Furthermore, in Fig. 7, the predicted velocity changes of the AUV at time steps during the transition from the spiral trajectory to the linear trajectory, specifically at $t = [349.8, 350.2]$, are depicted. The graph illustrates that stability constraint is satisfied by guaranteeing that the predictions converge to zero at the end

of the prediction horizon.

2) Case 2: Two test scenarios are considered to demonstrate the capability of the proposed controller to track trajectories containing unreachable points. The reference trajectory $\mathbf{y}^d(k)$ is defined by two straight lines, in the $xy-$pane, with no changes in the $z-$direction. In Test 1, no vehicle positional constraints are applied; therefore, the reference trajectory $\mathbf{y}^d(k)$ is regarded as reachable and doesn't consider workspace constraint. In Test 2, the workspace is constrained by $|x| \leq 16$ and $|y| \leq 25$, which makes part of the reference stay outside the constrained region.

The plots of time profiles of the position outputs and control inputs in both Test 1 and Test 2 are shown in Fig. 8. To make the convergence properties of the proposed MPC visible, the response in the $xy-$plane is shown in Fig. 9 along with the implemented output constraints. Evidently, the
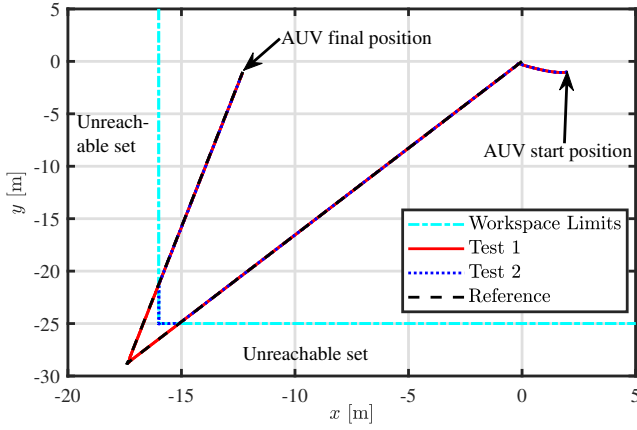
Fig. 9. Case 2: Closed-loop motion of the AUV in the $x - y$ plane with the impact of unreachable reference signals demonstrated.

result of Test 1 is as expected because the outputs tracked the desired trajectories throughout the simulation range. In Test 2, there are unreachable points along the defined trajectories due to the workspace constraints, which deviates the AUV movement from the reference until the desired trajectories become reachable. Based on the reference calculation in (20), it is expected that the AUV will converge to the optimum values within the reachable set $\mathcal{R}_{\mathcal{Y}}$, $i.e.$, the optimum points that correspond to the boundaries defined by the intersecting vertical and horizontal constraint lines.

V. CONCLUSIONS AND FUTURE WORKS

This paper presents a velocity form model predictive controller for combined 3D trajectory tracking and point stabilisation control of an AUV operating in the presence of ocean current and wave disturbances. The ocean current is modelled to move at a constant speed while the ocean waves are modelled as time-varying disturbances with both primary and secondary components of the waves considered. The main control objective is to minimise tracking errors when the AUV is steered to follow a reachable, and possibly unreachable, 3D reference trajectory. This control objective is achieved with input and state constraints considered in the optimisation design. The designed predictive controller also achieves close-to-zero errors in the 6 DoFs of the vehicle in point stabilisation, as required for effective docking operation. The constraint on the pitch angle is imposed to prevent the rotation matrix from becoming singular. The control input constraints are a result of the limits on the forces and moments that the vehicle can generate, and the upper velocity bounds are usually required for a variety of underwater tasks. The closed-loop stability is guaranteed by enforcing a terminal equality constraint.

The simulation results demonstrate the merit of the proposed control algorithm. Importantly, it shows that offset-free control is useful for minimising output tracking errors in both time-varying reference tracking and point stabilisation. Moreover, state augmentation that is a feature of velocity-based techniques is avoided to prevent any increased computational

demand. In the future development, the proposed methodology can be expanded to consider collision-avoidance control in the presence of fixed or moving obstacles. The experimental validation in laboratory environment is another next-step work. Moreover, the issue of lacking guaranteed robust stability in offset-free tracking MPC remains open.

APPENDIX

A. Dynamic Parameters Description

- $\mathbf{M} = \mathbf{M}_{\mathrm{RB}} + \mathbf{M}_{\mathrm{AM}} \in \mathbb{R}^{6 \times 6}$ is the inertia matrix consisting of two matrices, with subscript 'RB' standing for rigid body and 'AM' for added mass components, defined explicitly as

$$\mathbf{M}_{\mathrm{RB}} = \begin{bmatrix} m & 0 & 0 & 0 & mz_g & -my_g \\ 0 & m & 0 & -mz_g & 0 & mx_g \\ 0 & 0 & m & my_g & -mx_g & 0 \\ 0 & -mz_g & my_g & I_{xx} & 0 & 0 \\ mz_g & 0 & -mx_g & 0 & I_{yy} & 0 \\ -my_g & mx_g & 0 & 0 & 0 & I_{zz} \end{bmatrix},$$

$$\mathbf{M}_{\mathrm{AM}} = - \begin{bmatrix} X_{\dot{u}} & 0 & 0 & 0 & 0 & 0 \\ 0 & Y_{\dot{v}} & 0 & 0 & 0 & Y_{\dot{r}} \\ 0 & 0 & Z_{\dot{w}} & 0 & Z_{\dot{q}} & 0 \\ 0 & 0 & 0 & K_{\dot{p}} & 0 & 0 \\ 0 & 0 & M_{\dot{w}} & 0 & M_{\dot{q}} & 0 \\ 0 & N_{\dot{v}} & 0 & 0 & 0 & N_{\dot{r}} \end{bmatrix},$$

where $\mathbf{r}_g^b = [x_g \ y_g \ z_g]^\top$, is the vector from the origin of the body-fixed coordinate system to the centre of gravity of the AUV expressed in the same reference frame. I_{xx}, I_{yy} and I_{zz} represent the moment of inertia. The added mass matrix component $X_{\dot{u}}$, represents the hydrodynamic added force X along the x-axis due to acceleration $\dot{u}$ in the x-axis. Similar notations are used for $y-$ and $z-$directions, on the other five acceleration terms, $\dot{v}$, $\dot{w}$, $\dot{p}$, $\dot{q}$ and $\dot{r}$. The entries in $\mathbf{M}_{\mathrm{RB}}$ and $\mathbf{M}_{\mathrm{AM}}$ are typically provided in AUV specifications.

- $\mathbf{C}(\boldsymbol{\nu}) = \mathbf{C}_{\mathrm{RB}} + \mathbf{C}_{\mathrm{AM}} \in \mathbb{R}^{6 \times 6}$ is the Coriolis-centripetal matrix with rigid body and added mass components. The rigid body component based on Lagrangian parameterisation is given by [7]:

$$\mathbf{C}_{\mathrm{RB}} = \begin{bmatrix} \mathbf{0}_{3 \times 3} \\ -m\mathbf{S}(\boldsymbol{\nu}_1) + m\mathbf{S}(\mathbf{r}_g^b)\mathbf{S}(\boldsymbol{\nu}_2) \\ -m\mathbf{S}(\boldsymbol{\nu}_1) - m\mathbf{S}(\boldsymbol{\nu}_2)\mathbf{S}(\mathbf{r}_g^b) \\ \mathbf{S}(\mathbf{I}_b\boldsymbol{\nu}_2) \end{bmatrix} \quad (28)$$

in which $\mathbf{I}_b = \mathrm{diag}(I_{xx}, I_{yy}, I_{zz})$. For convenience, the inertia matrix is written in a block structure as

$$\mathbf{M}_{\mathrm{AM}} = \begin{bmatrix} M_{11} & M_{12} \\ M_{21} & M_{22} \end{bmatrix}. \quad (29)$$

The added mass Coriolis effects based on skew-symmetrical parameterisation is written as

$$\mathbf{C}_{\mathrm{AM}} = \begin{bmatrix} \mathbf{0}_{3 \times 3} & -\mathbf{S}(M_{11}\boldsymbol{\nu}_1 + M_{12}\boldsymbol{\nu}_2) \\ -\mathbf{S}(M_{11}\boldsymbol{\nu}_1 + M_{12}\boldsymbol{\nu}_2) & -\mathbf{S}(M_{21}\boldsymbol{\nu}_1 + M_{22}\boldsymbol{\nu}_2) \end{bmatrix}.$$

where $\boldsymbol{\nu}_1 = [u \ v \ w]^\top$ and $\boldsymbol{\nu}_2 = [p \ q \ r]^\top$.

- $\mathbf{D}(\boldsymbol{\nu}) \in \mathbb{R}^{6 \times 6}$ is the vehicle's hydrodynamic damping matrix. The Naminow-D AUV model adapted in this

work employs a coupled structure and nonlinear representation of the damping effects such that $\mathbf{D}(\boldsymbol{\nu}) = -\mathbf{D}|\boldsymbol{\nu}|$, where

$$\mathbf{D} = \begin{bmatrix} X_{|u|u} & 0 & 0 & 0 & 0 & 0 \\ 0 & Y_{|v|v} & 0 & 0 & 0 & Y_{|r|r} \\ 0 & 0 & Z_{|w|w} & 0 & Z_{|q|q} & 0 \\ 0 & 0 & 0 & K_{|p|p} & 0 & 0 \\ 0 & 0 & M_{|w|w} & 0 & M_{|q|q} & 0 \\ 0 & N_{|v|v} & 0 & 0 & 0 & N_{|r|r} \end{bmatrix},$$

in which $X_{|u|u}, \cdots, N_{|r|r}$ are the nonlinear hydrodynamic coefficients and $|\boldsymbol{\nu}|$ denotes the absolute value of the velocity vector

- The vector $\mathbf{g}(\eta) \in \mathbb{R}^{6 \times 1}$ describes the forces and moments due to the AUV's weight and buoyancy, i.e.,

$$\mathbf{g}(\eta) = \begin{bmatrix} (W - B)\sin\theta \\ -(W - B)\cos\theta\sin\phi \\ -(W - B)\cos\theta\sin\phi \\ -g_y\cos\theta\sin\phi + g_z\cos\theta\cos\phi \\ g_z\sin\theta + g_x\cos\theta\cos\phi \\ -g_x\cos\theta\sin\phi - g_y\sin\theta \end{bmatrix},$$

where $g_x = (x_gW - x_bB)$, $g_y = (y_gW - y_bB)$ and $g_z = (z_gW - z_bB)$. Here, the vector $[x_b \ y_b \ z_b]^\top$ denotes the centre of of buoyancy of the AUV and is assumed to coincide with the centre of gravity, while W and B are the weight and buoyancy of the AUV, respectively.

B. Proof of Theorem 1

This proof is given in three steps. Step I establishes recursive feasibility and Step II shows that the proposed control strategy provides closed-loop stability. In step III, it is shown that offset-free control is ensured for reachable piece-wise constant references. For reference signals that are not reachable, the algorithm converges to a reachable point that minimises the tracking error. The first two steps follow the standard approach in MPC literature with some modifications to suit the current study.

Step I: Given that the initial state increment $\Delta\mathbf{x}(k|k) = \Delta\mathbf{x}(0)$ is feasible, the optimal control sequence from solving (22) is $\{\Delta\boldsymbol{\tau}(k|k)^*, \Delta\boldsymbol{\tau}(k+1|k)^*, \ldots, \Delta\boldsymbol{\tau}(k+N_u-1|k)^*\}$. Shifting the current time by 1 so that $k \leftarrow k + 1$ results in a feasible and possibly sub-optimal solution given by $\{\Delta\boldsymbol{\tau}(k+1|k)^*, \ldots, \Delta\boldsymbol{\tau}(k+N_u-1|k)^*, \mathbf{0}\}$ obtained by setting $\Delta\boldsymbol{\tau}(k+N_u|k)^* = \mathbf{0}$, which also implies $\boldsymbol{\tau}(k+N_u|k)^* = \boldsymbol{\tau}(k+N_u-1|k)^*$. Based on the constraint $\Delta\boldsymbol{\nu}(k+N|k) = \mathbf{0}$, keeping the input unchanged for a constant reference $\mathbf{y}_s^d$, makes the terminal state $\mathbf{x}(k+N|k) = \mathbf{x}_r(k)$, a forced equilibrium at steady state and is feasible. For curved or time-varying user-defined reference signals $\mathbf{y}^d(k)$, the constraint ensures $\mathbf{x}(k+N|k)$ is a feasible state since $\mathbf{r}(k)$ is reachable for all k.

Step II: Let $V(k)$ be equal to the cost function evaluated at time k. We note that the cost function is always positive and equal to zero only when $|\mathbf{y}(k+j|k) - \mathbf{r}(k)| = 0$ and $\Delta\boldsymbol{\tau}(k+i|k) = 0$. To guarantee (Lyapunov) stability, we now need to show that $V(k)$ decays monotonously. Considering the feasible input increment sequence at time step $k + 1$ constructed in *Step I*, a feasible, possibly suboptimal, value

of the cost function $V(k + 1)$ expressed in terms of $V(k)$ is given by

$$\begin{aligned} V(k + 1) = V(k) &- \| \mathbf{y}(k+1|k) - \mathbf{r}(k) \|_{\mathbf{Q}}^2 - \| \Delta\boldsymbol{\tau}(k|k) \|_{\mathbf{R}}^2 \\ &+ \| \mathbf{y}(k+N|k) - \mathbf{r}(k) \|_{\mathbf{Q}}^2 \end{aligned}$$
(30)

From (30), it is straightforward to see that the forcing of $\mathbf{y}(N+1|k)$ to be equal to $\mathbf{r}(k)$ through the stability constraint ensures that $\| \mathbf{y}(k+N|k) - \mathbf{r}(k) \|_{\mathbf{Q}}^2 = 0$. This implies $V(k + 1) \leq V(k)$ holds because $\| \mathbf{y}(k+N|k) - \mathbf{r}(k) \|_{\mathbf{Q}}^2 - \| \mathbf{y}(k+1|k) - \mathbf{r}(k) \|_{\mathbf{Q}}^2 - \| \Delta\boldsymbol{\tau}(k|k) \|_{\mathbf{R}}^2 \leq 0$, and the only condition that will enable the equality to hold is when the system reaches steady state with $\mathbf{y}^d(k) = \mathbf{y}_s^d$ and $\Delta\boldsymbol{\tau}(k|k) = \mathbf{0}$ as $k \rightarrow \infty$. In sum, $V(k)$ is a Lyapunov function that decreases along the prescribed trajectories. Thus, the predictive controller is asymptotically stable given $\mathbf{r}(k) \ \forall k$.

Step III Here, we follow an approach similar to that used in [42] where constraints are assumed inactive at steady state which means that the predictive control law can be considered unconstrained. Under the assumption of piece-wise constant reference, $\mathbf{y}^d(\infty) = \mathbf{y}_s^d$ and $\mathbf{d}(k) \rightarrow \mathbf{d}(\infty)$ at steady state when the vehicle converges towards the docking point. The stability of the closed-loop system at steady state implies that $\mathbf{x}(k) = \mathbf{x}(\infty)$, $\mathbf{y}(k) = \mathbf{y}(\infty)$ and $\boldsymbol{\tau}(k) = \boldsymbol{\tau}(\infty)$ as $k \rightarrow \infty$.

First consider the case where $\mathbf{y}_s^d \in \mathcal{R}_{\mathcal{Y}}$. In this case, the steady state reachable reference $\mathbf{r}(\infty) = \mathbf{y}_s^d$ because it minimises (20) and fulfills the properties of $\mathcal{R}_{\mathcal{Y}}$ with $\lambda = 1$. Assume that the predictive controller (22) is unconstrained at this steady state. For this unconstrained case, it is evident that the optimal control increment is given by

$$\Delta\boldsymbol{\tau}^*(\infty) = \mathbf{K}_{MPC}(\mathbf{r}(\infty) - \mathbf{y}^0(\infty)) \tag{31}$$

where $\mathbf{K}_{MPC}$ is the unconstrained controller gain and $\mathbf{y}^0(\infty)$ is the "free" trajectory which represents the part of $\mathbf{y}(\infty)$ that depend on the past control and the actual measurement *i.e.,* without terms in $\Delta\mathbf{U}_k^*$ to be computed. Based on the system convergence, $\Delta\boldsymbol{\tau}^*(\infty) = 0$ which means that $\mathbf{y}^0(\infty) = \mathbf{r}(\infty)$ holds from (31). Furthermore, $\mathbf{y}^0(\infty) = \mathbf{y}(\infty)$ because $\mathbf{y}(k-1) = \mathbf{y}(k) = \mathbf{y}(\infty)$ as $k \rightarrow \infty$. Therefore, the system converges to $\mathbf{y}_s^d$, *i.e.,* the plant output reaches the reference because $\mathbf{y}^0(\infty) = \mathbf{r}(\infty) \implies \mathbf{y}(\infty) = \mathbf{y}_s^d$ at steady state and this ensures offset-free control.

For the second case in which $\mathbf{y}_s^d \notin \mathcal{R}_{\mathcal{Y}}$, The vector $\mathbf{r}(\infty)$ that minimises (20) is not exactly equal to $\mathbf{y}_s^d$, that is, $\mathbf{r}(\infty) \neq \mathbf{y}_s^d$. However, $\mathbf{r}(\infty)$ can take any arbitrary reachable output that minimises (20) while ensuring it remains in the same set $\mathcal{R}_{\mathcal{Y}}$ as the current steady state reachable output $\mathbf{y}(\infty)$. Following similar procedure under the assumption of unconstrained law as in the first case, it follows that the closed-loop system converges with $\mathbf{y}(k) = \mathbf{r}(k) \neq \mathbf{y}_s^d$ as $k \rightarrow \infty$. Hence, completing the proof.

REFERENCES

[1] A. Sahoo, S. K. Dwivedy, and P. Robi, "Advancements in the field of autonomous underwater vehicle," *Ocean Eng.*, vol. 181, pp. 145–160, 2019.

[2] J. Yuh, "Design and control of autonomous underwater robots: A survey," *Autonomous Robots*, vol. 8, no. 1, pp. 7–24, 2000.

[3] T. I. Fossen, *Guidance and Control of Ocean Vehicles*. John Wiley & Sons, Chichester, England, 1994.

[4] Z. Dong, L. Wan, Y. Li, T. Liu, J. Zhuang, and G. Zhang, "Point stabilization for an underactuated AUV in the presence of ocean currents," *Int. J. Adv. Robot. Syst*, vol. 12, no. 7, p. 100, 2015.

[5] X. Xiang, L. Lapierre, C. Liu, and B. Jouvencel, "Path tracking: Combined path following and trajectory tracking for autonomous underwater vehicles," in *2011 IEEE/RSJ Int. Conf. Intell. Robot. Syst.* IEEE, 2011, pp. 3558–3563.

[6] C. Shen and Y. Shi, "Distributed implementation of nonlinear model predictive control for AUV trajectory tracking," *Automatica*, vol. 115, p. 108863, 2020.

[7] T. I. Fossen, *Handbook of Marine Craft Hydrodynamics and Motion Control*. John Wiley & Sons, 2011.

[8] F. Repoulias and E. Papadopoulos, "Planar trajectory planning and tracking control design for underactuated AUVs," *Ocean Eng.*, vol. 34, no. 11-12, pp. 1650–1667, 2007.

[9] A. P. Aguiar and A. M. Pascoal, "Dynamic positioning and way-point tracking of underactuated AUVs in the presence of ocean currents," *Int. J. Control*, vol. 80, no. 7, pp. 1092–1108, 2007.

[10] B. Huang, B. Zhou, S. Zhang, and C. Zhu, "Adaptive prescribed performance tracking control for underactuated autonomous underwater vehicles with input quantization," *Ocean Eng.*, vol. 221, p. 108549, 2021.

[11] X. Liang, X. Qu, N. Wang, R. Zhang, and Y. Li, "Three-dimensional trajectory tracking of an underactuated AUV based on fuzzy dynamic surface control," *IET Intell. Transp. Syst.*, vol. 14, no. 5, pp. 364–370, 2020.

[12] Y. Li, C. Wei, Q. Wu, P. Chen, Y. Jiang, and Y. Li, "Study of 3 dimension trajectory tracking of underactuated autonomous underwater vehicle," *Ocean Eng.*, vol. 105, pp. 270–274, 2015.

[13] Z. Yan, H. Yu, W. Zhang, B. Li, and J. Zhou, "Globally finite-time stable tracking control of underactuated UUVs," *Ocean Eng.*, vol. 107, pp. 132–146, 2015.

[14] J. Guerrero, J. Torres, V. Creuze, and A. Chemori, "Trajectory tracking for autonomous underwater vehicle: An adaptive approach," *Ocean Eng.*, vol. 172, pp. 511–522, 2019.

[15] L. Qiao and W. Zhang, "Adaptive non-singular integral terminal sliding mode tracking control for autonomous underwater vehicles," *IET Control Theory Appl*, vol. 11, no. 8, pp. 1293–1306, 2017.

[16] J. Guo, F.-C. Chiu, and C.-C. Huang, "Design of a sliding mode fuzzy controller for the guidance and control of an autonomous underwater vehicle," *Ocean Eng.*, vol. 30, no. 16, pp. 2137–2155, 2003.

[17] P. S. Londhe and B. Patre, "Adaptive fuzzy sliding mode control for robust trajectory tracking control of an autonomous underwater vehicle," *Intell. Serv. Robot*, vol. 12, no. 1, pp. 87–102, 2019.

[18] B. Sun, D. Zhu, and W. Li, "An integrated backstepping and sliding mode tracking control algorithm for unmanned underwater vehicles," in *Proc. 2012 UKACC.* IEEE, 2012, pp. 644–649.

[19] L. Yu, H. Chaohuan, and M. Xiaochuan, "Backstepping based integral sliding mode control for autonomous underwater vehicles," in *32nd Proc. CCC.* IEEE, 2013, pp. 5438–5442.

[20] H. N. Esfahani, B. Aminian, E. I. Grøtli, and S. Gros, "Backstepping-based integral sliding mode control with time delay estimation for autonomous underwater vehicles," in *20th ICAR.* IEEE, 2021, pp. 682–687.

[21] C. Yang, F. Yao, and M.-J. Zhang, "Adaptive backstepping terminal sliding mode control method based on recurrent neural networks for autonomous underwater vehicle," *Chin. J. Mech. Eng-en*, vol. 31, no. 1, pp. 1–16, 2018.

[22] J. Zhou, X. Zhao, T. Chen, Z. Yan, and Z. Yang, "Trajectory tracking control of an underactuated AUV based on backstepping sliding mode with state prediction," *IEEE Access*, vol. 7, pp. 181 983–181 993, 2019.

[23] C. Shen, Y. Shi, and B. Buckham, "Trajectory tracking control of an autonomous underwater vehicle using lyapunov-based model predictive control," *IEEE Trans. Ind. Electron.*, vol. 65, no. 7, pp. 5796–5805, 2017.

[24] J. M. Maciejowski, *Predictive control: with constraints*. Prentice Hall. Harlow, England, 2002.

[25] E. F. Camacho and C. Bordons, "Nonlinear model predictive control," in *Model Predictive control*. Springer, 2007, pp. 249–288.

[26] P. Jagtap, P. Raut, P. Kumar, A. Gupta, N. Singh, and F. Kazi, "Control of autonomous underwater vehicle using reduced order model predictive control in three dimensional space," *IFAC-PapersOnLine*, vol. 49, no. 1, pp. 772–777, 2016.

[27] S. Heshmati-Alamdari, G. C. Karras, P. Marantos, and K. J. Kyriakopoulos, "A robust predictive control approach for underwater robotic vehicles," *IEEE Trans. Control Syst. Technol.*, vol. 28, no. 6, pp. 2352–2363, 2019.

[28] S. Heshmati-Alamdari, A. Nikou, and D. V. Dimarogonas, "Robust trajectory tracking control for underactuated autonomous underwater vehicles in uncertain environments," *IEEE Trans. Autom. Sci. Eng.*, vol. 18, no. 3, pp. 1288–1301, 2020.

[29] C. Shen, B. Buckham, and Y. Shi, "Modified C/GMRES algorithm for fast nonlinear model predictive tracking control of AUVs," *IEEE trans. Control Syst. Technol.*, vol. 25, no. 5, pp. 1896–1904, 2016.

[30] W. Naeem, R. Sutton, and S. Ahmad, "Pure pursuit guidance and model predictive control of an autonomous underwater vehicle for cable/pipeline tracking," in *Proc. World Maritime Technol. Conf., San Francisco, CA, USA*, 2003, pp. 1–15.

[31] Y. Zhang, X. Liu, M. Luo, and C. Yang, "MPC-based 3-D trajectory tracking for an autonomous underwater vehicle with constraints in complex ocean environments," *Ocean Eng.*, vol. 189, p. 106309, 2019.

[32] H. Uchihori *et al.*, "Linear parameter-varying model predictive control of AUV for docking scenarios," *Appl. Sci.*, vol. 11, no. 10, p. 4368, 2021.

[33] L. Wang, *Model predictive control system design and implementation using MATLAB®*. Springer Science & Business Media, 2009.

[34] I. A. Jimoh, I. B. Küçükdemiral, G. Bevan, and P. E. Orukpe, "Offset-free model predictive control: a study of different formulations with further results," in *MED2020.* IEEE, 2020, pp. 671–676.

[35] P. S. Cisneros and H. Werner, "A velocity algorithm for nonlinear model predictive control," *IEEE Trans. Control Syst. Technol.*, vol. 29, no. 3, pp. 1310–1315, 2020.

[36] K. R. Muske and J. B. Rawlings, "Linear model predictive control of unstable processes," *J. Process Control*, vol. 3, no. 2, pp. 85–96, 1993.

[37] Z. Yan, P. Gong, W. Zhang, and W. Wu, "Model predictive control of autonomous underwater vehicles for trajectory tracking with external disturbances," *Ocean Eng.*, vol. 217, p. 107884, 2020.

[38] E. Borhaug, A. Pavlov, and K. Y. Pettersen, "Integral LOS control for path following of underactuated marine surface vessels in the presence of constant ocean currents," in *Proc. IEEE CDC.* IEEE, 2008, pp. 4984–4991.

[39] G. Betti, M. Farina, and R. Scattolini, "A robust MPC algorithm for offset-free tracking of constant reference signals," *IEEE Tran. Autom. Control*, vol. 58, no. 9, pp. 2394–2400, 2013.

[40] L. Wang, "A tutorial on model predictive control: Using a linear velocity-form model," *Dev. Chemical Eng. Miner. Process.*, vol. 12, no. 5-6, pp. 573–614, 2004.

[41] S. Gros, M. Zanon, R. Quirynen, A. Bemporad, and M. Diehl, "From linear to nonlinear MPC: bridging the gap via the real-time iteration," *Int. J. Control*, vol. 93, no. 1, pp. 62–80, 2020.

[42] U. Maeder, F. Borrelli, and M. Morari, "Linear offset-free model predictive control," *Automatica*, vol. 45, no. 10, pp. 2214–2222, 2009.

[43] I. A. Jimoh, I. B. Küçükdemiral, and G. Bevan, "Fin control for ship roll motion stabilisation based on observer enhanced MPC with disturbance rate compensation," *Ocean Eng.*, vol. 224, p. 108706, 2021.